Design Rules for the Nano-Bio Interface of Nanodiamonds: Implications for siRNA Vectorization

Marek Kindermann, Jitka Neburkova, Eva Neuhoferova, Jan Majer, Miroslava Guricova, Veronika Benson, Petr Cigler

Design Rules for the Nano-Bio Interface of Nanodiamonds: Implications for siRNA Vectorization

*Marek Kindermann, Jitka Neburkova, Eva Neuhoferova, Jan Majer, Miroslava Guricova, Veronika Benson and Petr Cigler**

M. Kindermann, Dr. J. Neburkova, J. Majer, Dr. M. Guricova, Dr. P. Cigler
Institute of Organic Chemistry and Biochemistry of the Czech Academy of Sciences
Flemingovo namesti 2, 166 10 Prague 6, Czech Republic
E-mail: cigler@uochb.cas.cz

M. Kindermann, E. Neuhoferova, Dr. V. Benson
Institute of Microbiology of the Czech Academy of Sciences
Videnska 1083, 142 20 Prague 4, Czech Republic

M. Kindermann
Department of Physical Chemistry
University of Chemistry and Technology Prague
Technicka 5, 166 28 Prague 6, Czech Republic

E. Neuhoferova
Faculty of Science
Charles University
Hlavova 2030, Prague 2, 128 40, Czech Republic

Keywords: nanodiamond, siRNA delivery, transfection, cationic copolymer

Abstract

The enormous therapeutic potential of selective RNA interference has recently been manifested by the approval of several small interfering RNA (siRNA)-based drugs. However, the efficacy of siRNA delivery is still limited, and an extensive search for alternative and highly effective delivery approaches is ongoing. With this aim, three generations of non-viral vectors based on modified nanodiamonds (NDs) have been gradually developed in the past decade. They show great promise due to the negligible toxicity of the ND core. Here, a robust methodological approach is presented to enable the evaluation of new vector nanomaterials. Using a new type of third-generation ND vector coated with a copolymer with tunable charge density, variables such as colloidal stability, surface electrostatic properties, the molecular composition of the copolymer and the mode of complexation with siRNA are optimized. Using an innovative data processing strategy, the results are related to biological potency, toxicity and cell proliferation. Finally, the optimized composition of a coating copolymer consisting of a cationic component, 2-dimethylaminoethyl methacrylate, and an electroneutral biocompatible component, *N*-(2-hydroxypropyl) methacrylamide, is evaluated. The optimized NDs vectors are colloidally and biologically stable siRNA delivery tools with broad potential for RNA interference-based therapeutics.

1. Introduction

RNA-based gene therapies have seen a rapid development in the last two decades and various types of RNA drugs reached their first clinical applications.[1,2] While the development of mRNA vaccines[3,4] has been critical for controlling the COVID-19 pandemic, RNA interference (RNAi) is increasingly being used to specifically silence gene expression at the post-transcriptional level. Recent efforts have led to the first regulatory approval of Onpattro, a small interfering RNA (siRNA)-based drug, in 2018,[5] followed by three drugs based on siRNA conjugates with *N*-acetylgalactosamine (GalNAc).[6–8] In addition to these, six other siRNA-based drugs are in late phase 3 clinical trials,[9,10] paving the way for wider use of RNAi-based therapy.

Nevertheless, the therapeutic application of siRNA is still in its infancy and requires extensive optimization. At the systemic level, naked siRNA molecules without additional modifications exhibit a low bioavailability associated with rapid clearance and degradation by nucleases.[9] Several clinical trials were terminated because of low efficacy or serious side effects as an unspecific immune response caused by the recognition of naked siRNA by the innate immune system.[11,12]

The common strategy of avoiding siRNA degradation, recognition by immune system and enabling to cross biological barriers is based on suitable delivery nanosystems protecting the fragile siRNA. Although the most promising strategies for siRNA delivery are currently based on lipid nanoparticles[13,14] and GalNAc-siRNA conjugates,[6–8] a wide range of delivery nanosystems (polymers, dendrimers, lipids, inorganic particles, viral vectors, etc.[15,16]) are being developed as viable alternatives.

Among these nanosystems, nanodiamonds (NDs) have been investigated as a potential siRNA delivery system in the past decade.[17–21] Two main types of NDs are used: detonation NDs (DNDs) and high-pressure high-temperature (HPHT) NDs, which differ in surface

chemistry, shape and size.[22,23] Primary DND particles have a diameter of several nanometers and are covered by amorphous carbon with mixed sp^2/sp^3 hybridization.[24] Their aqueous dispersion typically contains small aggregates with a broad particle size distribution.[25] In addition to their potential use as siRNA vectors,[17,20] DNDs have been proven, for example, to be long-term stable carriers providing antimicrobial activity[26,27] and as highly selective binders of fibroblast growth factors.[25,28]

By contrast, HPHT NDs provide additional features such as fluorescence from nitrogen vacancy centers, which enables the imaging, tracking and dynamic reporting of the physical and molecular processes surrounding NDs using quantum optical approaches.[29–34] HPHT NDs are, however, a covalent crystalline material that is essentially non-biodegradable. Due to their characteristic size, typically >10 nm in diameter,[25,35] HPHT NDs cannot be excreted *via* the renal pathway, and is therefore probably not suitable for routine systemic administration. On the other hand, no significant toxicity[22,36,37] has been observed for HPHT NDs, which makes this material promising for locoregional[38] and topical applications.

Compared to soft/organic carriers, solid inorganic nanoparticles (NPs) require more demanding surface modification to control their colloidal properties.[39,40] Without a proper modification, NDs aggregate under physiological conditions due to the high ionic concentration (see **Figure S6** in Supporting information). This makes the design of the surface coating (surface charge density, structure, molecular flexibility, hydrophilicity, chemical composition, etc.) crucial in the preparation of inorganic NP systems providing a compelling performance in biological systems.[39–41] Specifically, for the complexation of negatively charged siRNA as well as for the colloidal stabilization of NPs, cationic coatings are required. **Figure 1** presents the various engineering strategies for creating cationic polymer coatings useful for siRNA delivery.

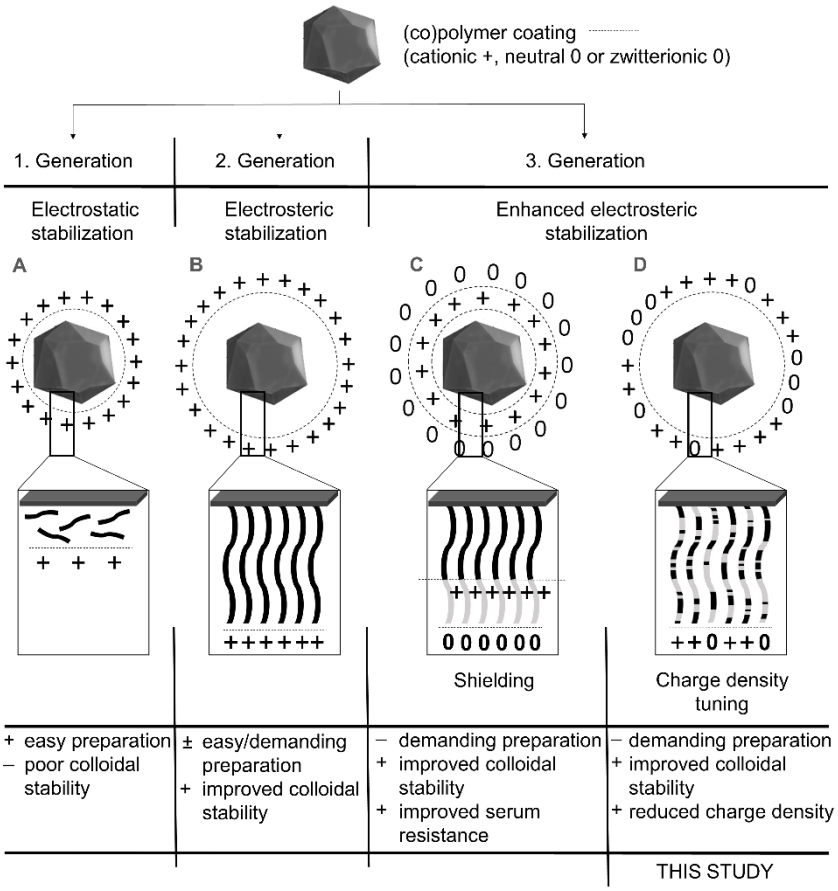

Figure 1. Scheme of various engineering strategies for the production of cationic polymer-coated NPs. Linear polymer chains represent only one example of many possible polymer structures (linear, branched, cross-linked, etc.[42]) Polymers can also be attached to the NP surface *via* different approaches (electrostatic interaction, covalent grafting or hydrophobic interaction).[39]

The first generation of coatings (Figure 1A) introduces electrostatic stabilization of NPs, which prevents their aggregation by repulsive electrostatic forces. This approach can be achieved by coating with coating using cationic polymers, for instance low molecular weight (0.8 kDa) branched polyethyleneimine (PEI),[18,43–46] or by hydrogenation of the surface.[21] The disadvantage of this approach is the high sensitivity of NPs to ionic strength. Because the physiological environment (including biological media such as PBS, cell culture medium etc.) typically possesses a high ionic strength reducing the thickness of the stabilizing electrical double layer around the NPs, dispersing such particles leads to their poor colloidal stability,

aggregation and limited biological availability.[47,48] Potentially, serum proteins can be used to stabilize such particles.[48]

To improve the colloidal stability of the previous generation of coatings, polymers of higher molecular weight are required. For example, 25 kDa branched PEI, ~30 kDa poly(L-lysine),[49] 6.9 kDa poly(amidoamine) (PAMAM dendrimer),[20] and poly(2-dimethylaminoethyl methacrylate) (PDMAEMA linear brush)[50] have been investigated. This second-generation (Figure 1B) interface covers the particle surface in such a way that the charged polymer chains extend out into the solution and provide additional steric stabilization, which is based on the micro-Brownian motion of the flexible ends of the polymer chains. This electrosteric stabilization[51] usually resists high ionic strength and provides sufficient stabilization in aqueous dispersants. However, the improved colloidal behavior is compromised by a greater cytotoxicity of the polymers, which increases with the increasing molecular weight of PEI,[52] poly(L-lysine),[53] PAMAM,[53] and PDMAEMA.[54] The transfection efficacies of these cationic polymers seem to be somewhat contradictory.[52,55–57] Despite ongoing efforts, the biological properties of polyplexes/cationic NPs are not fully understood because of the complex dependence of biological activity on physicochemical properties such as polymer structure, molecular weight, buffer capacity, charge density, the degree of DNA/RNA complexation, colloidal stability, polydispersity, and the tendency to form a protein corona.[55]

The third generation of coatings (Figure 1C, 1D) was developed specifically for transfections in biological dispersants. Interactions of serum components with a cationic interface can strongly affect the colloidal stability and effectivity of siRNA delivery.[11] To avoid nonspecific adsorption of serum components, polymer shells with shielding molecules have been designed, for instance poly[ethylene glycol]-*block*-poly[2(dimethylamino)ethyl methacrylate-*co*-butyl methacrylate] (PEG-*b*-poly(DMAEMA-*co*-BMA)),[58] PEI-PEG,[59] and poly[2-(dimethylamino) ethyl methacrylate]-*block*-poly[*N*-(3-(methacryloylamino)propyl)-*N*,*N*-dimethyl-*N*-(3-sulfopropyl)ammonium hydroxide] (PDMAEMA-*b*-PMPDSAH).[60] The

shielding parts are exposed to the solution, allowing effective colloidal protection (Figure 1C). The cationic components can also be conjugated to the "supporting" hydrophilic layer of the polymer; for example, basic polypeptides (Arg_8, Lys_8, and His_8) are covalently attached to a poly(glycerol) layer on the particles.[61] Furthermore, serum proteins adsorbed on the surface can improve cellular uptake by acting as endogenous targeting ligands interacting with cellular receptors instead of a synthetic interface.[62,63] On the other hand, it has also been shown that the opsonization effect results in uptake by the reticuloendothelial system, followed by phagocyte mediated clearance.[9,64]

Among other parameters, the toxicity of cationic transfectants is associated with their high charge density.[57,65] In the present work, we demonstrate a systematic approach to the design, synthesis, colloidal, and *in vitro* evaluation of a cationic (co)polymer interface on HPHT NDs with tunable charge density (third generation, Figure 1D). We base the cationic coating on 2-dimethylaminoethyl methacrylate ($PDMAEMA^+$). This polymer can be used for siRNA transfection in free form[66] or as an ND coating[50] (of the second generation), but it also shows a significant cytotoxicity.[66] To potentially improve and optimize the overall biological performance of the ND particles coated with $PDMAEMA^+$, we introduced an *N*-(2-hydroxypropyl) methacrylamide ($HPMA^0$) component into the structure of the surface coating to reduce the charge density. Poly[*N*-(2-hydroxypropyl) methacrylamide] ($PHPMA^0$)[67] is a hydrophilic biocompatible and antifouling polymer which has been used in various polymer-drug conjugates.[68] In previous works[29,41,69–72] we demonstrated that $PHPMA^0$ can be used advantageously for diamond coating and colloidal stabilization.

Here, we investigate a poly($DMAEMA^+$-*co*-$HPMA^0$) coating of NDs consisting of a statistically copolymerized cationic ($DMAEMA^+$) and an electroneutral, hydrophilic ($HPMA^0$) component. We analyze in detail the effect of the increasing amount of the $HPMA^0$ component in the cationic copolymer to elucidate the relationship between the physicochemical properties and biological activity of these vector systems. We study the colloidal stability of coated NDs

in biological conditions and optimize their complexation with siRNA using multiple techniques. We analyze the cytotoxicity of the complexes and their efficiency of *in vitro* gene silencing in cells of the mouse 4T1 breast cancer line.

2. Results and Discussion

Design, composition, and synthetic approach: NDs bearing a covalently grafted cationic (co)polymer with tuned positive charge density offer a novel approach to siRNA vectorization. We took advantage of our recently published methodology for silica coating of NDs[40] to prepare a cationic linear-brush (co)polymer layer. Terminally attached methacrylate groups on a silica coating allowed the growth of a dense poly(DMAEMA^{+}-*co*-HPMA^{0}) layer directly from the surface *via* radical polymerization (**Figure 2**).

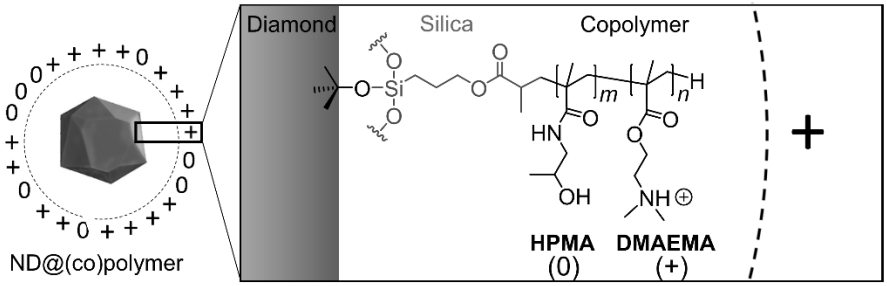

Figure 2. Schematic structure of the cationic (co)polymer coating on the ND surface.

We used "grafting though" radical polymerization[73] where the polymerizable methacrylate groups are first anchored onto the nanoparticle surface. The polymerization is initiated in a solution containing dissolved methacryloylated nanoparticles and free monomers. The methacrylates pre-attached on the surface are gradually integrated into the growing polymer chains. The "grafting through" method differs from the "grafting from" method, where functional initiators are chemically linked onto the nanoparticle surface to directly initiate the polymerization.[74] Nevertheless, both methods typically ensure a denser and better-protecting

coating than the attachment of pre-synthesized polymers (PEI,[43] poly-L-lysine,[49] PEG,[75] etc.) to the surface as in the "grafting to" approach.[39]

Characterization of the HPHT-ND@(co)polymer: We prepared ND particles coated with ND@silica@poly[DMAEMA(x%)$^{+}$-*co*-HPMA(y%)^{0}] (co)polymers of various compositions, abbreviated in the following text as DMAEMA(x%)$^{+}$/HPMA(y%)^{0}: $100^{+}/0^{0}$, $80^{+}/20^{0}$, $45^{+}/55^{0}$, $33^{+}/67^{0}$, $0^{+}/100^{0}$, or in general represented as ND@(co)polymer; the "(co)polymer" notation reflects sample series comprising particles coated with a homopolymer ($100^{+}/0^{0}$ and $0^{+}/100^{0}$) or copolymer ($80^{+}/20^{0}$, $45^{+}/55^{0}$, $33^{+}/67^{0}$). The numerical ratios describe the final percentage mass fraction of each monomer in the (co)polymer layer ($100^{+}/0^{0}$, DMAEMA^{+} only; $0^{+}/100^{0}$, HPMA only) – **Table S1** in the Supporting Information. To distinguish the resulting polarity of the apparent ζ-potential for nanoparticles after complexation with siRNA (ND@(co)polymer:siRNA), we similarly used the notation DMAEMA(x%)$^{+}$/HPMA(y%)^{0}(±) as follows: $100^{+}/0^{0}$:siR(−), $100^{+}/0^{0}$:siR(+), $80^{+}/20^{0}$:siR(+) and $45^{+}/55^{0}$:siR(+), where (+) sign reflects positive and (−) sign negative apparent ζ-potential (see section *Biological Testing*). The resulting (co)polymer composition was characterized by thermogravimetric analysis (TGA) and ^{1}H nuclear magnetic resonance (NMR) (**Figure 3**).

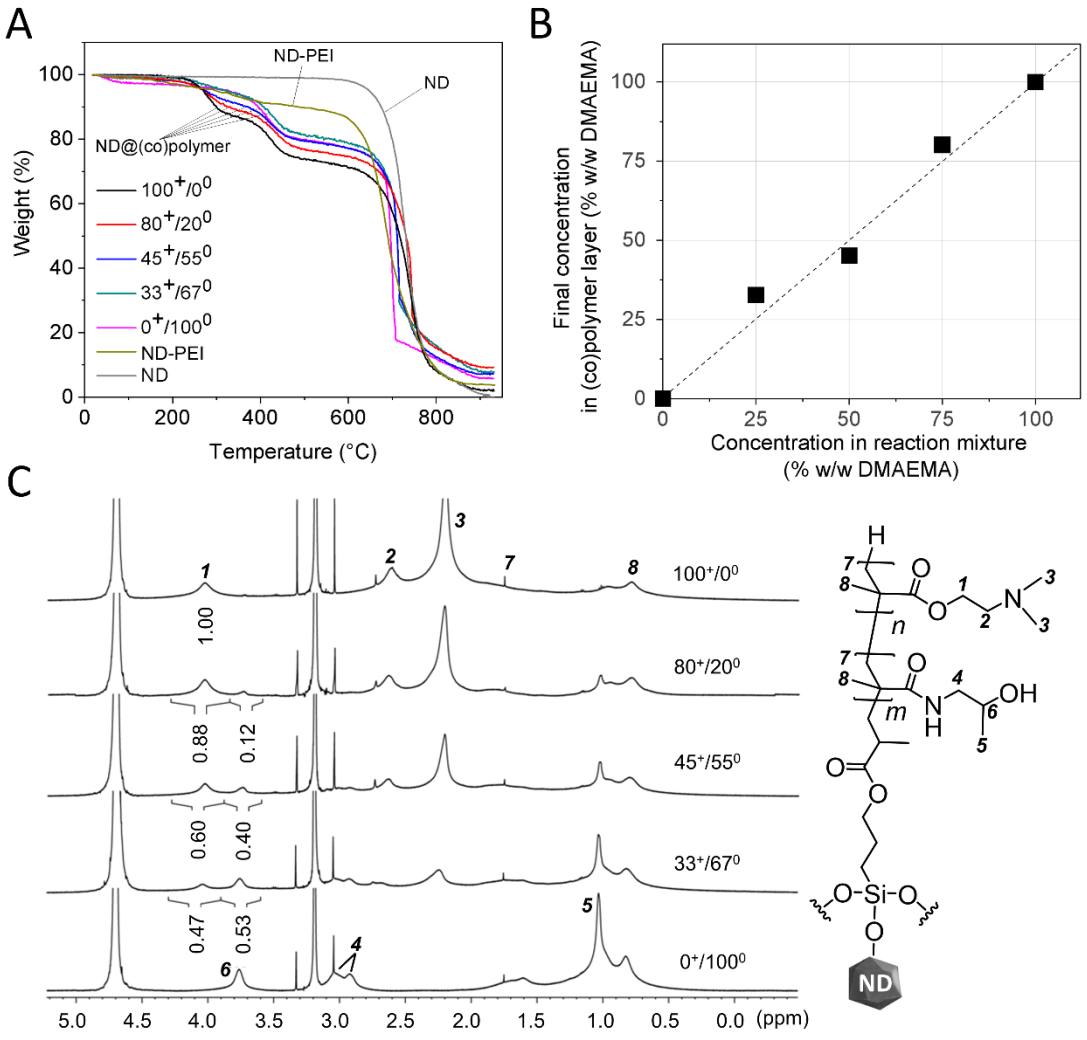

Figure 3. Characterization of ND@(co)polymer samples. A) TGA curves of ND, ND-PEI and ND@(co)polymer samples. B) Dependence of the copolymer composition in ND@(co)polymer samples on the composition of the reaction mixtures based on ^{1}H NMR data. C) ^{1}H NMR spectra of ND@(co)polymer samples. The structural assignment of the numbered peaks ***1-8*** is indicated in the scheme on the right.

The relation of the copolymer composition in ND@(co)polymer samples on the composition of the reaction mixture was estimated from ratios of the integral intensities of signals ***1*** (assigned to the hydrogens of the –O–C**H**$_2$– group in DMAEMA^{+}) and ***6*** (–C**H**–OH group in HPMA^{0}) in ^{1}H NMR spectra (Figure 3C). We found a linear dependence between the monomeric composition of the reaction mixture and the final composition of the polymer (Figure 3B).

The TGA results suggest, however, that the polymerization yields can increase slightly with the higher fraction of the cationic component (Figure 3A; based on the increasing relative weight loss of the (co)polymer from the $0^{+}/100^{0}$ to $100^{+}/0^{0}$ particles). Correspondingly, the dynamic light scattering (DLS) and nanoparticle tracking analysis (NTA) results obtained for the same particle series show an increasing size of the particles with the increasing fraction of the cationic component (**Table S7** and **S8** in the Supporting Information). Considering the similar size of the nanodiamond core, which was 37.8 ± 1.1 nm for all (co)polymer-coated samples (the mean value of their transmission electron microscopy (TEM) median diameters; Table S5 and **Figure S4** in Supporting information), all these data support a slightly positive influence of the cationic monomer on the polymerization yield. However, one has to consider that the measured hydrodynamic DLS and NTA sizes also reflect a swelling effect of the charged linear chains and restricted diffusion of charged particles due to the low ionic strength of water. Both factors typically contribute to the increase in measured size.

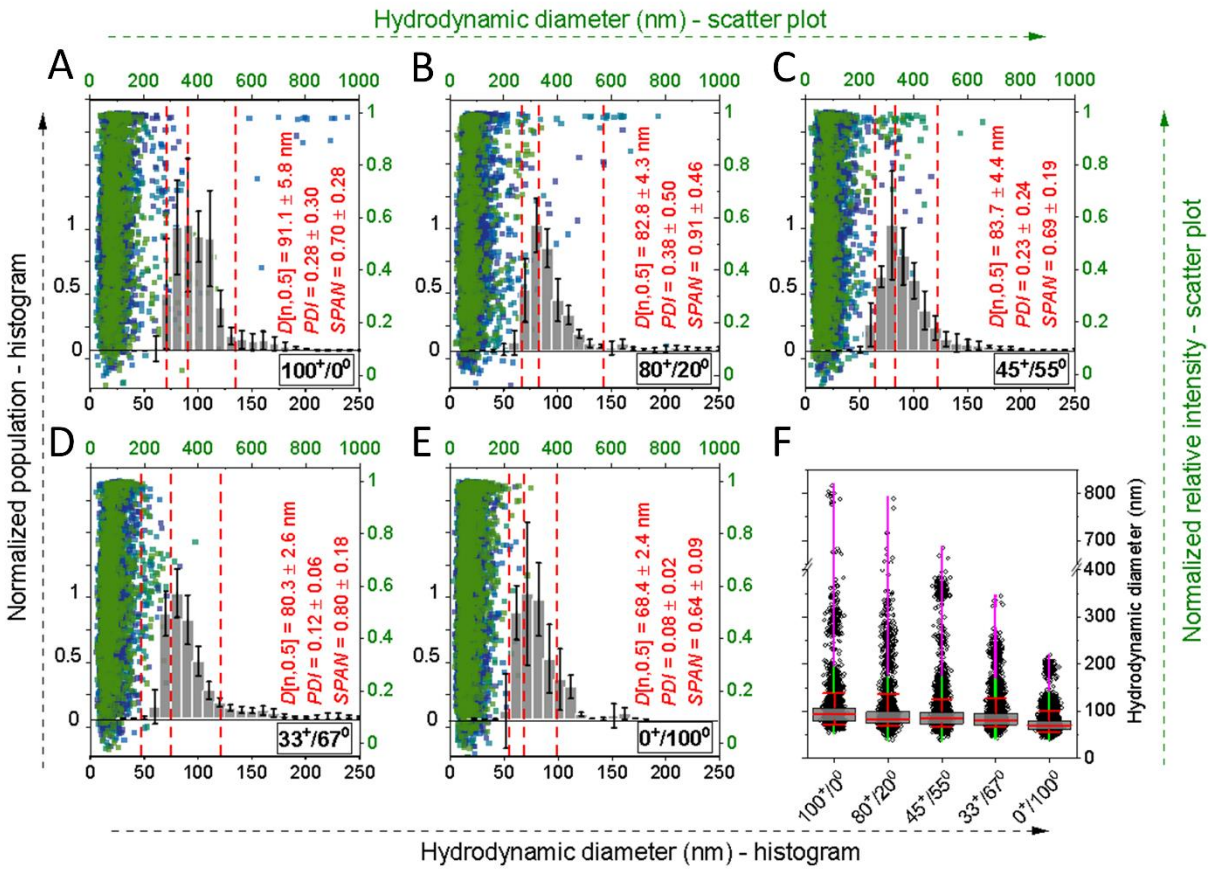

Figure 4. NTA measurement of ND@(co)polymer samples in water. The displayed finite track-length adjusted (FTLA) histograms (A, B, C, D, E) all represent data from five measurements of the same batch/sample ± standard deviation. Vertical red dashed lines coupled with the histograms represent the 10^{th}, 50^{th} (D[n,0.5]) and 90^{th} percentiles of the size distribution; *PDI* and *SPAN* values reflecting polydispersity were calculated from FTLA non-merged data (provided by software) according to equations (10) and (11) in Table S5. All valid tracks from the five measurements (raw data; manual data processing is described in the Experimental Section) are plotted in a scatter plot; each measurement is shown in a different color. F) Box plots characterizing the particle size distribution (five measurements) using the 25^{th}, 50^{th} and 75^{th} percentiles, and 90% and 10% whiskers; the horizontal red line in the box: median of the distribution; points surrounding the vertical green line: outliers defined as 3× the interquartile range (*IQR*) > outliers > 1.5×*IQR*; points surrounding the vertical magenta line: extreme values > 3×*IQR*. A MATLAB routine was applied to un-bin the FTLA data provided by software and to construct the box plots.

NTA and DLS results (**Figure 4** and **Figure S2** in the Supporting Information) revealed a higher degree of polydispersity (considering sensitive *PDI* values) and a tendency to form aggregates as the fraction of $DMAEMA^+$ in the (co)polymer grows. Although the DLS intensity-based results indicated a significant difference between the (co)polymer variants (see Table S5), the NTA results (Figure 4) clearly showed that this difference was given by the extreme values in the size distributions (Figure 4F). The mean value of the NTA median diameters over all (co)polymer-coated samples, 81.7 ± 7.3 nm, corresponds well with the mean value over all DLS number-weighted median diameters of 81.3 ± 11.6 nm. A detailed discussion focused on comparing the NTA, DLS and TEM results can be found in the corresponding section of the Supporting Information and in Table S5. The presence of these extreme values was probably caused by an interaction via surface patches of silica-coated particles not completely covered by (co)polymer layer, which do not reflect the average surface characteristics.[76] The measured electrophoretic light scattering (ELS) based apparent ζ-potentials of all (co)polymer compositions containing cationic $DMAEMA^+$ possess positive values from +35 to +42 mV. Only the PHMPA sample ($0^+/100^0$) exhibited slightly negative apparent ζ-potential −11 mV (see **Table S6** in the Supporting Information). Despite the uncharged PHPMA coating of

sample $0^{+}/100^{0}$, the underlying particle is likely not completely masked: The resulting apparent ζ-potential is influenced by both the silica-coating (negative charge of uncondensed silanol groups) and the polymer coating, as theoretically estimated for core-shell systems with thin polymer layers.[77]

The ζ-potential of (co)polymer-coated particles (denoted as "apparent") reported in this study is of relative meaning because we do not consider the presence/properties of the soft layer or the size of the particles when converting measured electrophoretic mobility.[77–79] The physical interpretation of apparent ζ-potential is therefore rather ambiguous. However, apparent ζ-potential remains a valuable tool for describing the interaction between particles, as shown in **Figure 5**.

HPHT-ND-PEI: properties and characterization: To compare the colloidal robustness of our novel system, we selected HPHT-ND-PEI (M_w ~0.8 kDa, branched) as a system belonging to the first generation of coatings. A proper colloidal characterization of HPHT-ND:PEI is still missing in the literature, but its colloidal properties definitely differ from those of DND:PEI complexes[43] due to the different size and surface chemistry of HPHT ND.[80] At first glance, fast and easy preparation of ND-PEI complexes was considered as an easy-to-use nano-tool for gene therapy[18,43,44] with promising *in vivo* results.[81] However, the colloidal stability of HPHT-ND-PEI complexes remains rather problematic.

We have observed that, in comparison with HPHT-ND@(co)polymer, this system suffers from (i) reversible aggregation during preparation, (ii) instability at high ionic strength, and (iii) colloidal aging resulting in aggregation. The procedure of mixing HPHT ND and PEI (0.8 kDa) typically resulted in an aggregated milky dispersion that flocculated. Centrifugation of the mixture and its transfer into water made it possible to remove the excess electrolytes and free PEI molecules and served us as a deflocculation process. Deflocculation restored the colloidal stability of ND-PEI complexes with a diameter of 107 nm (DLS Z-average) and apparent ζ-

potential of +28 mV (Table S6). However, subsequent stability testing in 10× PBS revealed immediate sample aggregation (Figure S6). Moreover, deflocculated ND-PEI without excess PEI at a concentration 9 mg mL^{-1}, stored in water for three days at 4 °C, underwent colloidal aging, which caused slow aggregation. Increased complex size of around 200 nm (DLS Z-average) was associated with an apparent ζ-potential reduction to −11 mV, likely due to the desorption of PEI molecules from the surface. Further centrifugation and washing of the stored sample with water resulted in the recovery of the diameter (108 nm, DLS Z-average), but subsequent time-dependent testing (~20 min) at room temperature revealed, again, slow aggregation with observable sedimentation.

Electrostatic complexation of siRNA onto cationic ND: Positively charged ND@(co)polymer NPs enabled complexation with siRNA *via* an electrostatic interaction providing ND@(co)polymer:siRNA complexes, which possess a positive or negative value of apparent ζ-potential. This interaction exhibited a typical mass ratio-dependent relationship[26] schematically represented in Figure 5.

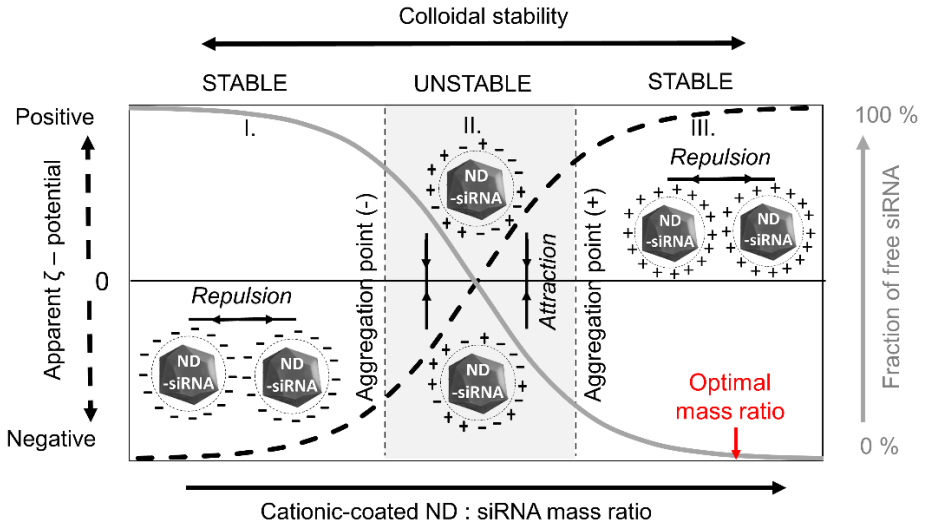

Figure 5. Schematic relationship between cationic-coated ND:siRNA mass ratio, apparent ζ-potential, fraction of free siRNA and colloidal stability of the ND:siRNA sample. The schematic graph is divided into three areas (marked as I, II and III) according to the colloidal

state of the sample (stable, unstable). The depicted curves are illustrative and do not represent real experimental data.

In general, all ND@(co)polymer:siRNA complexes tend to be colloidally stable at a mass ratio (ND:siRNA) of 20:1 or higher in water possessing a positive value of ζ-potential (Figure 5, area III). Aggregation at lower mass ratios (<20:1) was observed once the apparent ζ-potential of ND@(co)polymer:siRNA complexes started to decrease from positive values to zero or became slightly negative (colloidally unstable area II). The aggregation of the colloidal dispersion in area II may be caused by an interaction of surface patches. In addition, siRNA molecules can be considered rigid biopolymers (length ~7 nm; ~14 kDa) that potentially contributes to colloidal destabilization *via* a bridging mechanism that is known for comparably sized biomolecules (~10–100 kDa);[76,82] this effect often depends on the type of biomolecule, its concentration and solution chemistry.[82] Further decreasing of the mass ratio leads to the restoration of colloidal stability associated with an increasing fraction of free siRNA and a switch of the apparent ζ-potential of complexes to negative values (colloidally stable area I). As expected, the colloidally unstable area was specific for each (co)polymer layer and depended on its composition. It is obvious that as the number of positive charges within the (co)polymer shell increases, a lower mass ratio can be reached before aggregation is observed (aggregation point (+)). Consistently, all ND@(co)polymer particles showed different aggregation points (+) **(Figure 6A):** $100^{+}/0^{0}$ (< 5:1; not shown), $80^{+}/20^{0}$(~5:1), $45^{+}/55^{0}$ (~10:1), $33^{+}/67^{0}$(~15:1), $0^{+}/100^{0}$ (intact). The aggregation point of $100^{+}/0^{0}$ (< 5:1) lies outside of the monitored range and $0^{+}/100^{0}$ particles do not electrostatically interact with siRNA, so aggregation was not observed at all.

In contrast to ND@(co)polymer:siRNA, the effective binding mass ratio of ND-PEI:siRNA was significantly higher and the apparent ζ-potential values for all monitored mass ratios were negative. The reason for such different behavior is given by the relatively low amount of PEI present on the ND surface **(**Figure 3A**)** compared to the ND@(co)polymer. Furthermore, PEI

non-covalently attached to the surface does not form a brush-type conformation which provides a 3D system interacting effectively with siRNA. Finally, the repeating unit of PEI is ethylamine, resulting in a close packing of amino groups. Coulombic repulsion of neighboring groups causes that the PEI protonation degree at pH 5 is only 45 %.[57,83] All these factors contribute to enormously high optimal mass ratios for PEI (higher then 120:1[18]).

For practical applications, it can be useful to define an "optimal mass ratio" that is closely related with the aggregation point (+) and has the following characteristics (see **Figure 5**): (i) maximal siRNA loading on the particle surface, (ii) minimal value of the mass ratio, which still keeps the complex in colloidally stable area III and (iii) the resulting complex exhibiting a positive ζ-potential. Lastly, we use the concept of optimal mass ratio for the characterization of biologically tested samples (section *Biological Testing*).

Stability testing of ND-siRNA in biological conditions: Long-term stability testing of all ND-siRNA complexes was performed in the full cell culture medium (9% FCS, 37 °C; Figure 6B) and in a full fetal calf serum (FCS) (90% FCS, 37 °C; Figure 6C) to approximate *in vitro* and *in vivo* conditions, respectively. The DLS results in the cell culture medium showed the same stability range of ND@(co)polymer particles as observed in water; however, the aggregation points (+) were slightly shifted due to the presence of serum components. The positive surface charge of NPs and high abundance of the serum albumins (isoelectric point < 5.5) most probably leads to nonspecific protein adsorption, which provides further stabilization of ND@(co)polymer:siRNA complexes. This stabilization effect was observed in typical cell culture media such as DMEM and RPMI (see **Figure S5** in Supporting information).

The samples tested in the full FCS exhibited slow sedimentation, except $0^{+}/100^{0}$, which was intact. Nevertheless, the (co)polymers $80^{+}/20^{0}$:siR and $100^{+}/0$:siR, with a high content of the cationic component, showed reasonable stability. By contrast, the sample $45^{+}/55^{0}$:siR in the full FCS exhibited particularly poor stability for all monitored ratios. Clearly, the simple "~1:1

combination" of DMAEMA^{+} and HPMA^{0} (45^{+}/55^{0}:siR) did not lead to the optimal connection of their inherent properties and rather negatively affected colloidal stability in harsh biological conditions. On the other hand, a further decrease of the fraction of the neutral component led to an improvement of the colloidal behavior of 33^{+}/67^{0}:siR, which was similar to that of 0^{+}/100^{0}:siR.

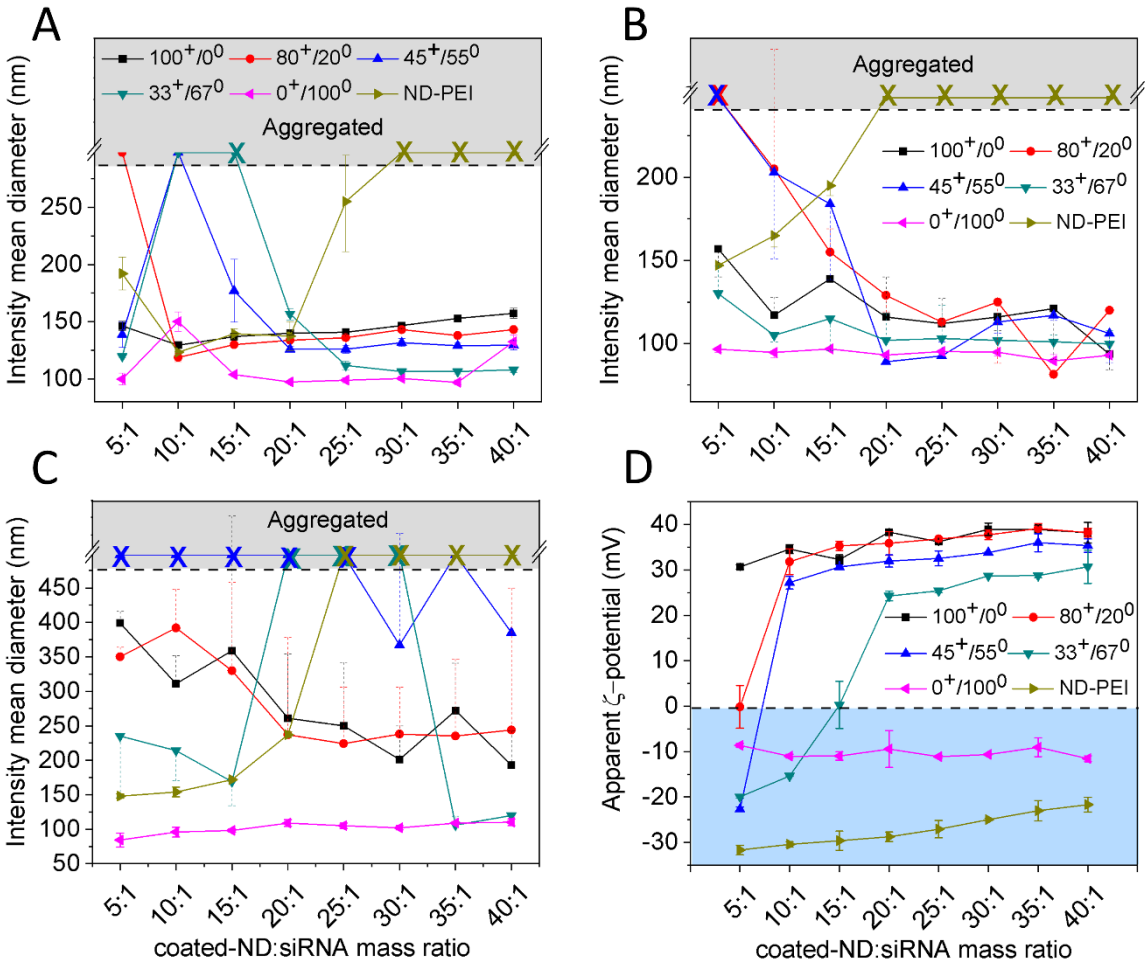

Figure 6. Colloidal properties of ND-PEI:siRNA and ND@(co)polymer:siRNA complexes at different mass ratios. DLS intensity weighted mean diameters (NNLS) of tested complexes A) in RNase-free water at 25 °C: Data points represent the mean value of intensity-weighted mean diameters ± sample standard deviation over three measurements of the same sample; B) in full cell culture medium for the 4T1 cell line (9% FCS) at 37 °C: Data points represent the first measurement of intensity mean diameter and the top/bottom part of the superimposed dashed line the 10th one (~ after 20 min); C) in full fetal calf serum (90% FCS) at 37 °C: The meaning of data points is the same as in B); D) Apparent ζ-potential in RNase-free water at 25 °C measured by electrophoretic light scattering (ELS).

Biological testing: To demonstrate the importance of a properly chosen optimal mass ratio, we tested two variants of the $100^{+}/0^{0}$:siR complex possessing opposite polarity of apparent ζ-potential: $100^{+}/0^{0}$:siR(+) and $100^{+}/0^{0}$:siR(−). In addition, we tested samples $100^{+}/0^{0}$:siR(+) and $80^{+}/20^{0}$:siR(+), because they revealed a similar stability trend in 90% FCS at 37 °C (see Figure 6D). Samples $33^{+}/67^{0}$ and $0^{+}/100^{0}$ with a low or zero content of cationic units were not considered promising because of their relatively high optimal mass ratios. The mouse 4T1 breast cancer cell line was utilized to perform the biological testing. Isolated total RNA, reflecting overall cell proliferation (**Figure 7A**), cellular cytotoxicity assessed using an LDH assay (**Figure S7**) and qPCR testing of the inhibition effect on the level of mouse GAPDH mRNA (Figure 7B, C) were measured to estimate the biological impact of the selected complexes.

The constant amount of bound siRNA for all tested samples caused that the increasing content of electroneutral monomer units in the (co)polymer layer was inherently connected with an increasing ND@(co)polymer:siRNA optimal mass ratio and an increasing NP concentration per well. The tested range of optimal mass ratios from 1:1 ($100^{+}/0^{0}$:siR(−)) to 20:1 ($45^{+}/55^{0}$:siR(+)) corresponds to 20–161 μg of ND@(co)polymer per well (see **Tables S3** and **S4** in Supporting information). Figure 7A, B shows a positive correlation between the reduction of cell proliferation and inhibition of GAPDH mRNA level as the number of particles per well/content of the neutral units in the (co)polymer layer increases. Aware of the limitations given by the *in vitro* experimental design (only one specific NP concentration was used for each coating type), it seems reasonable to expect that the increasing number of particles per well represents the dominant explanatory factor. In other words, it does not seem likely that particles containing a higher content of neutral units provide a better inhibition efficacy/cause stronger cell growth inhibition than more cationic complexes at a given NP concentration.

The inhibition effect size (percentage values in Figure 7C) was assessed from the dataset shown in Figure 7B by a Gaussian regression model in a Bayesian framework, which utilizes our

preliminary qPCR data as prior information for the analysis. Compared to the widely adopted frequentist approach (characterized e.g. by *p*-values), whose performance at small sample sizes is questionable, Bayesian estimates remain valid for any sample size; the price for this versatility, however, is dependence upon prior information.[84] One of the main tasks of the regression model (applied to the qPCR *dCt* values that allow comparison between the treatment groups) is to estimate a mean *dCt* value ($\overline{dCt}$) for a given treatment. The inherent feature of the Bayesian inference is to provide not only one estimate of the $\overline{dCt}$ value for given treatment, but rather a set (distribution) of $\overline{dCt}$ values with different relative plausibilities (see Figure 7C). To provide a reasonable comparison between the treatments, we calculated overlaps between the posterior distributions for given treatments (percentage values in Figure 7C).

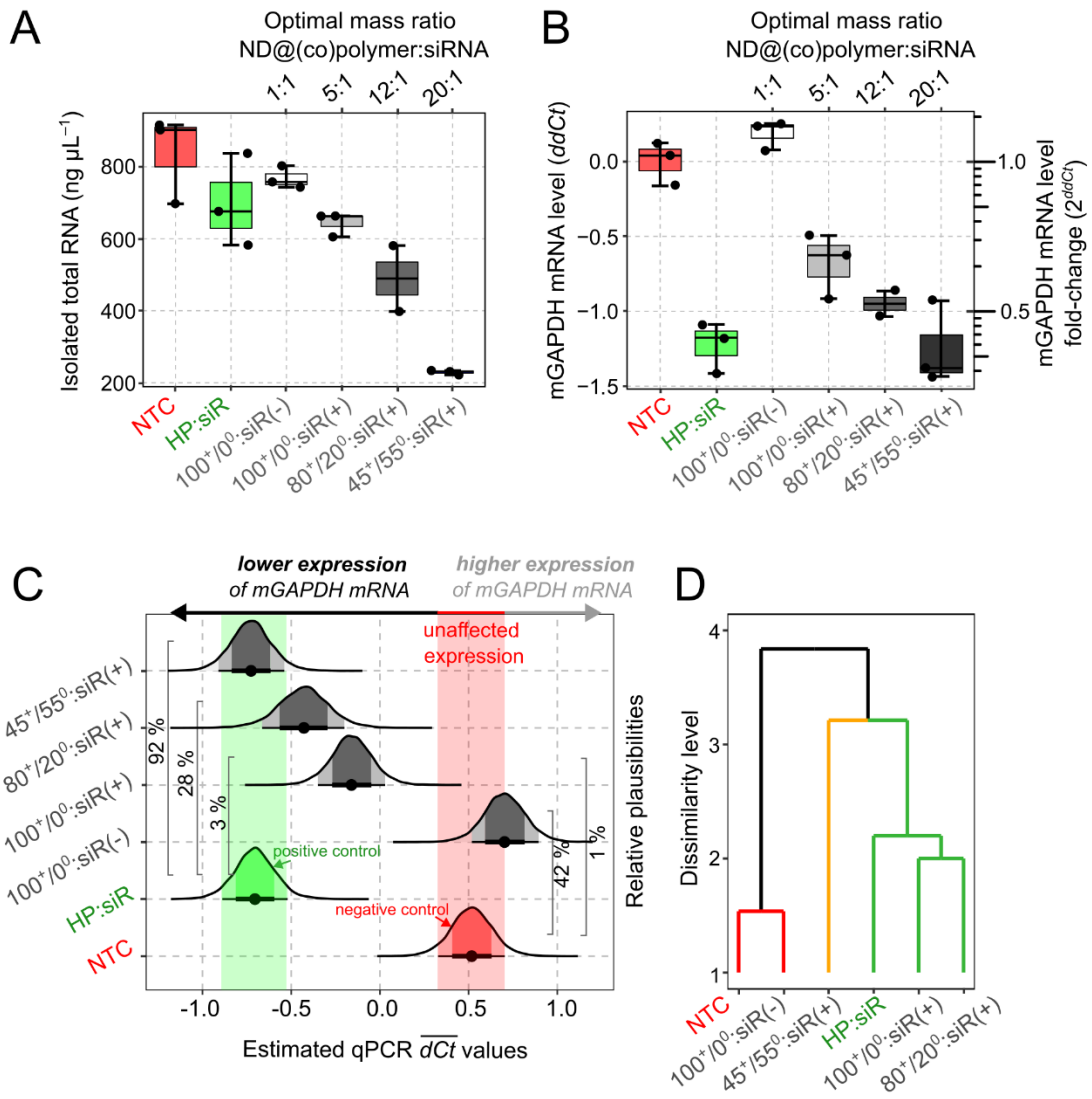

Figure 7. *In vitro* testing of ND@(co)polymer:siRNA complexes; the NTC represents a non-treated control and HP:siR is a positive control (commercial transfection agent). A) Overall cell proliferation represented by the amount of isolated total RNA (48 h after stimulation) from 4T1 cells before qPCR analysis. B) Inhibition of mouse GAPDH mRNA expression in 4T1 cells using 560 nM siRNA (final siRNA concentration in the well), measured by qPCR 48 h after stimulation; right y-axis is $\log_2$ scaled and 2^{ddCt} values reflect approximated fold change in gene expression defined by equation (5). For (A) and (B), the boxplot characterizes a sample using the 25^{th}, 50^{th} and 75^{th} percentiles; the upper/lower whisker extends from the hinge to the largest/smallest value (neither outliers nor extreme values are present in the data). C) Posterior relative plausibilities of qPCR $\overline{dCt}$ values for given treatment; inhibition effect size on mGAPDH mRNA expression is defined as an overlap between posterior relative plausibilities for given treatments (percentage values); dark circle shows the mean of the distribution; shaded areas under the posterior curves show 67% and 89% quantile intervals; red and green bands indicate 89% quantile intervals. Posterior estimates were inferred from a Bayesian Gaussian regression model. D) Cluster dendrogram of averaged biological replicates for isolated total RNA and qPCR *ddCt* values based on an Euclidean metric.

Data analysis shows a noticeable overlap (42 %) for posterior estimates $100^{+}/0^{0}$:siR(−) and non-treated control. Taking into account the overall position of the $100^{+}/0^{0}$:siR(−) posterior distribution (approximately half of its mass lies above the 89% quantile interval of the posterior for negative control) these results are most compatible with no important effect. Comparison of posterior overlaps for complexes with positive apparent ζ-potential and the positive control (HP:siR) shows an increasing degree of overlap as the NP concentration grows. Sample $45^{+}/55^{0}$:siR(+) with a concentration of 161 μg of the ND@(co)polymer per well reached a comparable inhibition effect (92% overlap) relative to the positive control. An acceptable biological effect, 28% overlap with positive control, was also observed for the sample $80^{+}/20^{0}$:siR(+). To provide an objective criticism of the analyzed dataset, it should be noted that the qPCR data are not fully independent since all biological replicates came from identical cell passage, and thus, narrowing overall variance.

Further analysis based on the agglomerative hierarchical clustering (a measure of dissimilarity between tested samples) of the data for isolated total RNA and GAPDH mRNA level revealed a separation of sample $45^{+}/55^{0}$:siR(+) from samples HP:siR, $100^{+}/0^{0}$:siR(+), $80^{+}/20^{0}$:siR(+) (see

Figure 7D). The applied NP concentration for $45^{+}/55^{0}$:siR(+) was as low as possible to complex the given amount of siRNA and keep the colloidal stability, however, an increased tendency of the cells to form clumps and lose adherence (Figure S3 in Supporting information) shows a limitation of this sample given by the low number of cationic units/high NP concentration. To obtain the optimal *in vitro* inhibition properties (effective gene inhibition without affecting cell viability), we proposed to use sample $80^{+}/20^{0}$:siR(+) resp. $100^{+}/0^{0}$:siR(+) with a mass ratio higher than the optimal one as shown in ref.[19] Besides that, the increased optimal mass ratio (25:1, $80^{+}/20^{0}$:siR(+)) was also applied for the treatment of xenografted Ewing sarcoma in mice.[19] This approach, however, would not be most likely advantageous for this particular cell line due to already reduced cell proliferation for sample $80^{+}/20^{0}$:siR(+) at an optimal ratio of 12:1. These results suggest that the system ND@(co)polymer:siRNA is not superior to the tested commercial control HP:siR for 4T1 cells. In our experience, the overall inhibition properties of ND@(co)polymer:siRNA complexes vary among different cell lines, e.g. well transfectable U-2 OS human bone osteosarcoma cells (effective inhibition without affecting cell viability) compared to HeLa human cervical adenocarcinoma cells where the gene inhibition was ineffective.[85]

In general, we did observe no cytotoxicity effects for any of the treatments presented (Figure S7 in Supporting information). On the other hand, cell proliferation was most likely affected by the applied optimal mass ratio/NP concentration. Obtained results also suggest the superiority of the samples with positive apparent ζ-potential compared to sample $100^{+}/0^{0}$:siR(−). Nevertheless, we want to emphasize that the polarity of the apparent ζ-potential cannot serve as a general parameter for assessing transfection capability, for example spherical nucleic acids[86,87] or HPHT-ND-PEI(0.8 kDa):antisense RNA[44,81] with a negative ζ-potential possess good transfection efficacy. By contrast, (3-aminopropyl) trimethoxysilane-terminated-detonation-ND:plasmid DNA complexes possessing positive potential do not elicit a sufficient

transfection response in comparison with detonation-ND-PEI(0.8 kDa):plasmid DNA,[43] which also has positive potential.

3. Conclusions

We have demonstrated a systematic approach to the synthesis and robust colloidal testing of a new vector nanosystem for siRNA delivery based on an ND core coated with the cationic (co)polymer poly(DMAEMA^{+}-*co*-HPMA^{0}). This system overcomes problematic colloidal properties of HPHT-ND-PEI complexes and effectively reduces the optimal binding ratio ND@coating:siRNA. Exploration of the ND@coating:siRNA optimal mass ratio is essential for the successful formulation of this charged nanoparticle system it should always be estimated before biological testing, including application-specific optimization. In our experience, assessment of the ratio is slightly batch-to-batch dependent and can depend on the siRNA provider (see ref.[19,85]). Overall, our results for the colloidal testing and vectorization of siRNA into mouse 4T1 breast cancer cells revealed a limited ability of the complexes containing a higher amount of neutral HPMA^{0} units to reach effective performance. Interestingly, a simple "~1:1 combination" of DMAEMA^{+} and HPMA^{0} (45^{+}/55^{0}-siR(+)) did not lead to the optimal connection of their inherent properties and rather negatively affected colloidal stability in biological conditions. The biological performance of ND@(co)polymer:siRNA complexes was not superior to the tested commercial control HP:siR for 4T1 cells.

In parallel with this study, the 80^{+}/20^{0}:siR(+) complexes have been utilized with various cell lines,[19,85,88] the treatment of xenografted tumors[19] and topical siRNA therapy of diabetic-like wounds.[88] Comparison of the 80^{+}/20^{0}:siR(+) vector system and HPHT-ND-PEI:siRNA elicited successful inhibition of the Ewing sarcoma EWS-FLI1 oncogene in cultured cells (inhibition of 90% compared to 55% obtained for PEI coating). The overall *in vitro* inhibition properties of the 80^{+}/20^{0}-siR(+)) complexes, however, vary among different cell lines: (i) the U-2 OS human bone osteosarcoma cells (high efficacy[85]), (ii) the 4T1 breast cancer cell line

(moderate efficacy, this study), and (iii) HeLa human cervical adenocarcinoma cells (poor efficacy[85]); all listed studies (i)-(iii) utilized siRNA sequence directed against GAPDH gen. The results of these studies suggest that the presented vector nanosystem deserves further exploitation, which is currently underway.

4. Experimental Section

Materials: Polyethyleneimine (PEI, MW = 800, branched), polyvinylpyrrolidone (PVP, MW = 10,000), tetraethyl orthosilicate (TEOS; always redistilled before use and stored under an argon atmosphere), 3-(trimethoxysilyl)propylmethacrylate (TMSPMA) and 2-dimethylaminoethyl methacrylate (DMAEMA), were purchased from Sigma–Aldrich. Aqueous ammonia (25% w/w) and ethanol (super-pure for UV, 96%) were purchased from Penta Chemicals (Czechia); methanol (gradient grade for HPLC, 99.9%) was supplied by VWR. *N*-(2-hydroxypropyl)methacrylamide (HPMA) was synthesized according to published procedures[89] and freshly recrystallized prior to use: 2.0 g HPMA was dissolved in 20 mL of ethyl acetate, gently heated to dissolve it in the solvent, filtered using a 0.2 μm polytetrafluorethylene (PTFE) microfilter, and hexane was added dropwise until HPMA precipitation initiated and then cooled in a freezer (−20 °C) for at least 2 h. 2,2'-Azobis(2-methylpropionitrile) (AIBN) was purchased from Sigma–Aldrich and freshly recrystallized prior to use: 1.3 g AIBN was dissolved in 65 mL of ethanol and recrystallized by thickening the ethanol solution on a rotary evaporator at a maximum temperature of 30 °C until crystallization initiated, then cooled down in a freezer (−20 °C) for at least 2 h. Duplexed mouse GAPDH siRNA (MW = 13968) with the following sequence was purchased from Sigma–Aldrich in the form of a desalted pellet:

sense strand: 5'-r(GAAGGUCGGUGUGAACGGAU)d(TT)-3'

antisense strand: 5'-r(AUCCGUUCACACCGACCUUC)d(TT)-3'.

The 4T1 cell line obtained from the ATCC (CRL-2539) was incubated in a full cell culture medium containing RPMI 1640 (Gibco) supplemented with 10% (v/v) fetal calf serum (FCS, Gibco), 44 mg L^{-1} gentamicin (Sandoz), 4.5 mg mL^{-1} glucose (Sigma–Aldrich), and 1.1% pyruvate (Sigma–Aldrich). Control transfection of GAPDH siRNA was carried out using the X-tremeGENE HP DNA Transfection Reagent (Roche) (complexes marked in the text as "HP:siR"). Total RNA was isolated using the RNeasy® Mini Kit (Qiagen) and reverse transcribed using random primers and the High Capacity cDNA Reverse Transcription Kit (Applied Biosystems). PCR quantification of cDNA was carried out with the gene-specific primers Mm99999915_g1 GAPDH (FAM, Life Technologies), Mm00437762_m1 B2M (FAM, Life Technologies) and a TaqMan Universal PCR Master Mix II, no UNG (Life Technologies). Cellular cytotoxicity was evaluated using an LDH assay (Roche). Unless stated otherwise, all reagents used in this work were used directly without further purification. Milli-Q water was used for all procedures and solutions if not stated otherwise.

ND Pretreatment: HPHT NDs were supplied by Microdiamant Switzerland (MSY 0–0.05). The NDs were oxidized by air in a furnace (Thermolyne 21100 tube) at 510 °C for 5 h. Subsequently, the NDs were treated with a mixture of H_2SO_4 and HNO_3 (9:1) at 90 °C for 3 days and washed with water, 1 M NaOH and 1 M HCl. They were washed an additional 5 times with water and then freeze-dried. Prior to use, the particles were dissolved in water (2 mg mL^{-1}) and sonicated with a probe (Cole–Parmer CPX 750, 20 kHz – tapered microtip 1/8" (3 mm)) – selected parameters: 30 min (ON-OFF cycle; 2 s ON, 2 s OFF), amplitude 40%. The resulting transparent colloid (ND) was incubated for 30 min at room temperature and filtered using a 0.2 μm polyvinylidene fluoride (PVDF) filter.

Coating of NDs with Methacrylate-terminated Thin Silica Layer (Part I): To avoid precipitation of ND during silication caused by increased ionic strength (ammonia), PVP was used as a

stabilizing dispersant.[39] PVP (187 mg, 0.0187 mmol) was dissolved in water (165 mL) and sonicated for 10 min in an ultrasonic bath (Ultrasonic Cleaner Elmasonic P60H, power 100%, 37 kHz, pulse mode). All samples sonicated in the ultrasonic bath were placed in a cavitation hotspot (see **Figure S1** in Supporting information). Unless stated otherwise, all coated ND samples after centrifugation were sonicated in a cup horn until they dissolved (Cole–Parmer CPX 750, 20 kHz – cup horn; samples were placed on the bottom of the cup) – selected parameters: amplitude 60%, duty cycle 100 %. ND colloid (33 mL, 2 mg mL^{-1}) was added, and the mixture was stirred for 24 h. The colloid was then concentrated by two-step centrifugation. In the first step (45,000*g*, 1 h), the mixture was centrifuged in 25 mL centrifuge tubes. The volume was reduced to approximately 22.4 mL. The second centrifugation step (30,000*g*, 30 min) was performed in microvials (16 × 1.4 mL), and the solvent volume was reduced to approximately 5 mL. Resuspended NDs were mixed with ethanol (96% v/v, 66 mL) in a round bottom flask during stirring. TEOS (495 μL, 2.22 mmol at 20 °C) and TMSPMA (165 μL, 0.694 mmol at 20 °C) were added to the round bottom flask during stirring and sonicated in an ultrasonic bath for 2–4 min. Aqueous ammonia (25% w/w, 2.75 mL, 37 mmol at 20 °C) was added and gently shaken. The reaction mixture was stirred for 14 h and then centrifuged in 25 mL tubes. The first centrifugation was done in three steps: first at 15,000*g* for 15 min, secondly, the supernatant was removed and centrifuged again at 20,000*g* for 20 min, and, lastly, the resulting supernatant from the second step was centrifuged at 50,000*g* for 20 min. The final supernatant was discarded and pellets were combined. The following centrifugations were performed in at least two steps – 25,000*g*, 25 min and 50,000*g*, 25 min. The sample was centrifuged five times and purified using methanol. The volume of the purified sample was reduced to approximately 2 mL by two-step centrifugation in 2 mL microvials (25,000*g*, 25 min and 50,000*g*, 25 min) and stored in a refrigerator (4 °C) overnight. Methacrylate-terminated ND nanoparticles in methanol were transferred into 414 μL of dimethyl sulfoxide (DMSO) using a rotary evaporator.

Coating of NDs with a (Co)polymer Layer (Part II): Different weight ratios of $DMAEMA^+$ (100, 75, 50, 25, 0 % w/w) and $HPMA^0$ (0, 25, 50, 75, 100 % w/w) were dissolved in 563 μL of DMSO (**Table S1** in the Supporting Information). The sample, prepared as 75 % $DMAEMA^+$/25 % HPMA ($80^+/20^0$ in text) in[19], was used. AIBN (56.4 mg, 0.343 mmol) was added to the mixture. The mixture was filtered using a 0.2 μm PTFE filter. Methacrylate-terminated NDs (prepared in *Part I*) in DMSO (57 μL, 9 mg of ND – considering 100% yield after silication) were added to each mixture. The rest of the methacrylate-terminated NDs (129 μL, 20 mg) were transferred into methanol (preventing hydrolysis of the silica layer) and stored at –20 °C. Vacuum degassing of the reaction mixture under argon filling cycles of the stirred mixture was performed (three cycles vacuum – argon, 1 min – 1 min using disposable 0.80×0.50 mm needles; appropriate degassing is important for successful polymerization). The degassed mixture reacted for 3 days under argon at 55 °C, after which the reaction was stopped by the addition of methanol. ND@(co)polymer samples were washed five times using RNase free water. Each washing step involved two centrifugations: 20,000*g* for 20 min and 40,000*g* for 20 min. The overall dilution factor was ~100×. Gravimetric analysis was performed to determine the sample concentration and final mass yield (see **Table S2** in Supporting information).

Coating of NDs with a PEI: PEI (100 μL, 0.9 mg mL^{-1}, 0.1 μmol) was dissolved in water and filtrated using a 0.2 μm PVDF filter; ND colloid (100 μL, 2 mg mL^{-1}) was added. The aggregated mixture was vortexed for at least 30 min and sonicated in an ultrasonic bath (power 100%, 37 kHz, pulse mode) which was filled with mixture of ice and water (the water-ice level in the bath was approximately 2.5 cm). Two-step centrifugation of the aggregated mixture was carried out; first 9,000*g* for 15 min then 30,000*g* for 15 min. Collected supernatants containing excess PEI were discarded and replaced with the same volume of water. The following

centrifugation (4×: 15,000*g*, 15 min and 30,000*g*, 15 min) and purification with RNase free water served as a deflocculation process resulting in transparent colloid ND-PEI; the final volume was 100 μL. Importantly, a pellet of ND-PEI after each centrifugation was dissolved in an ultrasonic bath hotspot (see Figure S1), not in the cup horn.

Complexation of siRNA for DLS, ELS Analysis and Qubit Assay: The siRNA stock solution was dissolved in RNase free water. Various amounts of the ND@(co)polymer (9 mg mL^{-1}) were diluted with RNase-free water, resulting in a final volume of 22.2 μL, and added into 2.8 μL (100 μM, 0.28 nmol, 3.91 μg) GAPDH siRNA (to reach the given ND@(co)polymer:siRNA mass ratio). The final mixture (25 μL or a scalable volume) was gently sonicated for 5-10 s in an ultrasonic bath, incubated at room temperature for 20 min and gently sonicated again. To obtain the desired concentration of ND@(co)polymer:siRNA complexes for further testing, the sample was centrifuged at 20,000*g* for 20 min and the necessary amount of supernatant was removed. The supernatant was analyzed using the Qubit miRNA assay kit to quantify the amount of free siRNA relative to the control (particle-free). Importantly, the quality of complexation of siRNA with cationic ND@(co)polymer depended on the commercial source of siRNA, likely because of the presence of remaining salts after purification.

Whereas siRNA from Sigma-Aldrich utilized in this study worked well, other siRNAs/DNAs from different sources typically led to the aggregation of the mixture. A significant increase of the ND@(co)polymer:siRNA mass ratio was required to fix this issue, for example from the optimal mass ratio 25:1 (Sigma-Aldrich) to 65:1 (Dharmacon); – this problem was also reported in.[19] *Short-term DLS/ELS testing* (**Figure 6A, C**): A dissolved ND@(co)polymer:siRNA pellet was added directly (not dropwise) into the RNase free water with the final volume of 0.6 mL. *Long-term DLS testing* (**Figure 6B, D**): Freshly prepared complexes of ND@(co)polymer:siRNA (final mixture, 25 μL) were mixed directly with the 4T1 cell culture medium (10% FCS) or with the 100% FCS (media containing FCS were centrifuged at 5,000*g*

for 10 min prior to use; the supernatant was used for measurements); dilution of the medium by the tested sample was always by ~10%; the particle concentration was in range from 0.07 mg mL^{-1} (5:1 coated-ND:siRNA mass ratio) to 0.34 mg mL^{-1} (40:1). The samples were preheated at 37 °C for 2 min, and mixed with a pipette before the analysis.

Cell Stimulation (Transfection Efficiency): The complexation procedure was upscaled to 50 μL (final volume) containing 5.6 μL (100 μM) of GAPDH siRNA, without further optimization (see *Complexation of siRNA for DLS, ELS Analysis and Qubit Assay* section). All ND samples for transfection were freshly prepared prior use and incubated at room temperature for approximately 60 min. A control transfection of GAPDH siRNA without NDs was carried out using 2 μL of X-tremeGENE HP DNA Transfection Reagent diluted by 42.4 μL of RNase free water and mixed with 5.6 μL (100 μM) GAPDH siRNA – HP:siR sample; prior to use, each sample was incubated for 20-30 min at room temperature.

ND Colloidal Stability Studies (DLS, ELS, NTA): Particle size distributions and average values of apparent ζ-potential were obtained using a Zetasizer Nano ZSP (Malvern Instruments). Intensity-weighted mean/median diameters were calculated from the second-order time intensity autocorrelation function $g^{(2)}(\tau)-1$ using a general purpose algorithm (NNLS) in Zetasizer Software 7.11. The intensity-weighted median diameters were calculated from the dominant (first) PSD peak. Z-average diameters were calculated from the fit by the first cumulant of a 3rd-order cumulant analysis. Data transformation into a number-weighted size distribution was also performed in Zetasizer Software using Mie theory without inspecting changes in optical properties due to (co)polymer coating; the real and imaginary part of the complex refractive index was set as 2.41 and 0.00 for nanodiamond samples, respectively; viscosity values for different dispersants can be found in **Table S7**; the dispersant refractive index was always set at 1.33 for all tested solvents. Data were collected at a backscatter angle

of 173° (NIBS system) using a quartz cuvette ZEN2112. In *short-term testing* (**Figure 6A, C**), each sample was measured three times with an automatic duration; reported size represents an average value of these measurements. In *long-term testing* (**Figure 6B, D**), each sample was measured ten times (approximately 20 min); viscosity values of utilized 90% FCS (100% full FCS diluted by tested sample) and 9% FCS (10% full cell culture medium for 4T1 cell line diluted by tested sample) at 37 °C were estimated as 0.861 cP[90] and 0.740 cP[91], respectively. These viscosity values characterize 100% FCS and cell culture medium (10% FCS); medium dilution was not reflected.

For the determination of the apparent ζ-potential, electrophoretic light scattering at a forward angle of 13° with a phase analysis of scattered light (PALS) was used. The apparent ζ-potential represents electrostatic potential calculated from electrophoretic mobility using the Smoluchowski approximation for spherical uncoated particles without considering the value of the ratio of particle size to Debye length. All samples were measured in RNase-free water using a disposable cuvette with a dip cell; monomodal analysis with two measurements and twenty subruns was chosen; the average sample conductivity was 41.3 μS cm^{-1} for all samples tested with siRNA. The complete ELS results are presented in Table S6. For both types of measurements, the particle concentration was lower than 0.1 mg mL^{-1} for the RNase-free solvent or 0.4 mg mL^{-1} for FCS or the full cell culture medium for the 4T1 cell line.

NTA measurements were performed with a Nanosight NS300 equipped with a low-volume cell connected to a linear pump and a 532 nm green laser (60 mW). Stock solutions of ND@(co)polymer NPs (9 mg mL^{-1}) were diluted in water with dilution factor of 10^5, resulting in measurements with 21-40 particles per frame and a number of valid tracks >930. The camera level was set to level 16 (shutter/gain: 1300/512), detected threshold to level 5 and syringe pump flow rate to level 12; blur, maximum jump distance and minimum expected particle size were set to “auto”. Each sample was measured 5 times for 60 s at ~25 °C. Captured data in “AllTracks.csv” files were analyzed manually; Measurements marked as FALSE (column:

"Included in distribution?") were excluded. Unique values in the column: "Particle ID" were found, and all repetitions were excluded. The final number of particles per measurement was equal to the number of valid tracks provided by software. Raw data, without applying finite track-length adjustment (FTLA), were plotted as a scatter plot (**Figure 4**) using data in the column "Ln(Adjusted intensity)/AU". NTA size distributions (**Figure 4**) are presented as normalized FTLA plots provided by software. Prior to use, all ND@(co)polymer samples were sonicated in a cup horn.

Electron microscopy (TEM): TEM experiments were performed with a JEOL JEM-1011 electron microscope operated at 80 kV equipped with a Tengra (EMSIS, Germany) bottom-mounted camera. Particles were placed on copper grids (Structure Probe, Inc., USA) with an in-house made parlodion membrane and carbon coating. A grid was pretreated with a droplet of poly(ethylenimine) solution (MW = 2.5 kDa, 0.1 mg mL^{-1}).[35] After 10 min of incubation, the droplet was removed with a piece of tissue, and the grid was placed on a droplet of deionized water for 1 min and dried once again. The grid was then placed on a droplet of an aqueous solution of the sample (0.1 mg/mL), the solution was removed with a piece of tissue after 3 min of incubation, and air-dried. In-house MATLAB code was used to implement semiautomatic segmentation of TEM images (MATLAB R2019b). Briefly, the Graph Cut technique (the Lazy Snapping algorithm[92]) was used in the Image segmenter app (*imageSegmenter*) to segment foreground and background regions. Segmented objects touching the image border were suppressed using the *imclearborder* function, and improperly identified objects were excluded from the image manually. Connected (8-connected) objects in the resulting binary image were labeled using *bwlable* function; properties (e.g. equivalent diameter) of labeled objects in the image were measured with the *regionprops* function. An object was labeled if it was either (i) a free-standing primary particle, or (ii) an aggregate composed of two or more primary particles; the inner structure of the aggregates was not considered. The particle statistic reflects labeled

objects from the image (each labeled object represents one particle included in the statistic). The equivalent diameter was calculated from the projected area of each labeled object.

Cell Culture and ND-siRNA Stimulation: The 4T1 cell line was stored in the full cell culture medium comprising 10% (v/v) DMSO at −80°C. On the first day (after thawing), the cells were incubated with a fresh full medium under a humid atmosphere containing 5% CO_2 (incubation conditions) overnight. On the second day, the full medium was changed and the cells were incubated for two days without changing the medium. On the fifth day, the cells (~250,000 cells mL^{-1} $well^{-1}$; determined using a Bürker counting chamber) were plated onto 12-well plates and incubated with fresh full medium overnight.

Transfection Efficiency – RNA Isolation, Reverse Transcription and Real-Time Quantitative RT-PCR (qPCR): On the sixth day, stimulation of the cells (confluence 70-80%) was performed; 50 µL of the sample was added dropwise and uniformly across the wells. The final volume per well was 1 mL (950 µL of full cell culture medium and 50 µL of testing sample dissolved in RNase free water); the amount of mouse GAPDH siRNA was constant for all samples (7.84 µg $well^{-1}$). More detailed information can be found in **Table S2** and **S3** in the Supporting Information. Stimulated cells were incubated for 48 h without changing the cell culture medium. All samples were analyzed in biological triplicates; all biological replicates were part of one single experiment (identical cell passage). The isolated total RNA fraction (5 µg; quantification using a NanoDrop™ 2000 instrument; the concentration was directly calculated from absorbance values at 260 nm) was reverse transcribed to cDNA. qPCR quantification was carried out with 2 µL of prepared cDNA. β-2-microglobulin (B2M) was used as an internal control for the quantitation of GAPDH expression. During qPCR, each biological replicate was analyzed as a technical triplicate for GAPDH and B2M using a Bio-Rad CFX Real Time PCR Detection System. Technical replicates were averaged and biological replicates

were analyzed statistically as independent measurements. Obtained cycle threshold (Ct) values were utilized to calculate dCt, $ddCt$ and 2^{ddCt} values for i^{th} biological replicate defined as:

$$dCt_i = Ct(\text{B2M})_i - Ct(\text{GAPDH})_i \quad (1)$$

$$\overline{dCt(\text{NTC})} = \frac{1}{3}\sum_{i=1}^{3} dCt(\text{NTC})_i \quad (2)$$

$$ddCt(\text{treat})_i = dCt(\text{treat})_i - \overline{dCt(\text{NTC})} \quad (3)$$

$$ddCt(\text{NTC})_i = dCt(\text{NTC})_i - \overline{dCt(\text{NTC})} \quad (4)$$

$$\text{fold change}_i = 2^{ddCt_i} = 2^{dCt_i - \overline{dCt(\text{NTC})}} = \frac{2^{dCt_i}}{2^{\overline{dCt(\text{NTC})}}}, \quad (5)$$

where $\overline{dCt(\text{NTC})}$ represents the mean value over biological triplicates, "treat" reflects samples HP:siR, $100^{+}/0^{0}$:siR(−), $100^{+}/0^{0}$:siR, $80^{+}/20^{0}$:siR(+) and $45^{+}/55^{0}$:siR(+), and NTC is the no-treatment control. The fold-change in gene expression (2^{ddCt}) has the meaning of a ratio between "sample relative expression" (2^{dCt}), and "mean relative expression" for NTC ($2^{\overline{dCt(NTC)}}$).

LDH Cytotoxicity Assay: Cells were seeded on 96-well plates (20,000 cells/well; 200 μL/well of a full medium supplemented with 1% serum) overnight. Biological triplicates were incubated with the ND complexes for 24 hours. A commercial lysis buffer was added to one triplicate of the control cells for the last 30 min of the experimental period (serving as an LDH assay positive control). The LDH assay was performed according to the manufacturer's instructions. Briefly, at the end of the experiment, the cell supernatant was collected and incubated with LDH dye for 10 min. Then the absorbance was measured with a reader using specific excitation at 490 nm and a reference excitation at 630 nm (Tecan spectrometer).

Other Analytical Methods: ^{1}H NMR spectra were recorded on a Bruker Avance III 500 spectrometer (499.88 MHz for ^{1}H and 125.71 MHz for ^{13}C) equipped with a 5 mm PFG

cryoprobe; 5 mg of each ND sample was centrifugated 3 times and transferred into D_2O, resulting in a final volume of approximately 50 μL. The signals were assigned by using a combination of 1D and 2D (H,H-COSY and H,C-HSQC) techniques. TGA was measured with a TG 750 Stanton Redroft instrument. A powder sample of approximately 1 mg was heated under air with a heating rate of 20 °C min^{-1}.

Statistical Analysis:

The inhibition effect of different siRNA treatments on 4T1 cells was assessed by a Gaussian regression model in a Bayesian framework (Figure 7C) using relevant software packages in R.[93–102] The Bayesian model defined below was fitted with the **brms** package,[101] which employs Stan software for probabilistic sampling.

$$\text{likelihood:} \qquad dCt_i \sim \text{Normal}(\mu_i, \sigma)$$

$$\text{linear model:} \qquad \mu_i = \beta_0 + \sum_{j=1}^{6} \beta_{1,\text{treat}_j} X_{i,\text{treat}_j}$$

$$\text{priors:} \qquad \beta_0, \beta_{1,\text{treat}_j} \sim \text{Normal}(mean = 0, sd = 2.0)$$

$$\sigma \sim \text{Student-t}(df = 3, lp = 0, sp = 2.5).$$

The first row shows a stochastic part of the model and states that the response variable *dCt* is a random variable independently drawn from a Gaussian distribution with mean μ and variance σ^2. The linear model in the second line describes how μ_i is constructed for given treatment. The remaining lines describe prior distributions; *sd* – standard deviation, *df* – degrees of freedom, *lp* – location parameter, *sp* – scale parameter. The **brms** package allows treating the model intercept (β_0) as just another β_{1,treat_j} parameter, and thus, makes no assumptions about centring. The weakly informative prior for β_{1,treat_j} is centered around 0 reflecting a

conservative assumption that $\overline{dCt(treatment)} - \overline{dCt(NTC)}$ might be positive ($\beta_{1,\mathrm{treat}_j} > 0$), negative ($\beta_{1,\mathrm{treat}_j} < 0$) or equal to zero ($\beta_{1,\mathrm{treat}_j} = 0$). The standard deviation (sd) of this prior was estimated from the preliminary qPCR data as $sd = 2 \times \text{standard deviation}(dCt)$; the preliminary study included only a no-treatment control and the positive control HP:siR; *sd* was calculated across all preliminary *dCt* values. A Markov chain Monte Carlo sampling procedure was performed with four chains that were run for 5000 iterations per chain, of which 2000 served as warm-up. Model diagnostics indicate a convergence of the sampling chains of the parameters (trace rank plot visual check, $\hat{R} = 1.00$, number of effective samples >3000). The full computer code, including more detailed model diagnostics and criticism (prior sensitivity analysis and posterior predictive check), is provided in an R Markdown document.

To construct the dendrogram (Figure 7D), data for isolated total RNA and qPCR *ddCt* values were standardized (z-scores were calculated); each biological replicate was represented by an average value over corresponding technical replicates. These standardized values were averaged over the biological replicates and agglomerative hierarchical clustering with an Euclidean metric was applied.

Acknowledgements

The authors are grateful to Dr. Martin Dracinsky (Institute of Organic Chemistry and Biochemistry of the Czech Academy of Sciences) for performing measurements and helping us with the analysis of ^{1}H NMR spectra, to Dr. Helena Raabova (Institute of Organic Chemistry and Bichemistry of the Czech Academy of Sciences) for her support of TEM measurements, and to Dr. Jaroslav Hanus (University of Chemistry and Technology Prague) for giving us access to the NanoSight NS300 system. This work was supported by the Czech Academy of Sciences – Strategy AV21 (VP29), and by the European Regional Development Fund; OP RDE; Project: CARAT (No. CZ.02.1.01/0.0/0.0/16_026/0008382) (to P.C.).

Conflicts of Interest

There are no conflicts to declare.

References

[1] Y.-K. Kim, *Exp. Mol. Med.* **2022**, *54*, 455.

[2] Y. Zhu, L. Zhu, X. Wang, H. Jin, *Cell Death Dis.* **2022**, *13*, 1.
[3] Y. N. Lamb, *Drugs* **2021**, *81*, 495.
[4] L. R. Baden, H. M. El Sahly, B. Essink, K. Kotloff, S. Frey, R. Novak, D. Diemert, S. A. Spector, N. Rouphael, C. B. Creech, J. McGettigan, S. Khetan, N. Segall, J. Solis, A. Brosz, C. Fierro, H. Schwartz, K. Neuzil, L. Corey, P. Gilbert, H. Janes, D. Follmann, M. Marovich, J. Mascola, L. Polakowski, J. Ledgerwood, B. S. Graham, H. Bennett, R. Pajon, C. Knightly, B. Leav, W. Deng, H. Zhou, S. Han, M. Ivarsson, J. Miller, T. Zaks, *N. Engl. J. Med.* **2021**, *384*, 403.
[5] T. Coelho, D. Adams, A. Silva, P. Lozeron, P. N. Hawkins, T. Mant, J. Perez, J. Chiesa, S. Warrington, E. Tranter, M. Munisamy, R. Falzone, J. Harrop, J. Cehelsky, B. R. Bettencourt, M. Geissler, J. S. Butler, A. Sehgal, R. E. Meyers, Q. Chen, T. Borland, R. M. Hutabarat, V. A. Clausen, R. Alvarez, K. Fitzgerald, C. Gamba-Vitalo, S. V. Nochur, A. K. Vaishnaw, D. W. Y. Sah, J. A. Gollob, O. B. Suhr, *N. Engl. J. Med.* **2013**, *369*, 819.
[6] A. D. Springer, S. F. Dowdy, *Nucleic Acid Ther.* **2018**, *28*, 109.
[7] M. M. Janas, C. E. Harbison, V. K. Perry, B. Carito, J. E. Sutherland, A. K. Vaishnaw, N. D. Keirstead, G. Warner, *Toxicol. Pathol.* **2018**, *46*, 735.
[8] Y. N. Lamb, *Drugs* **2021**, *81*, 389.
[9] M. M. Zhang, R. Bahal, T. P. Rasmussen, J. E. Manautou, X. Zhong, *Biochem. Pharmacol.* **2021**, 114432.
[10] I. S. Padda, A. U. Mahtani, M. Parmar, In *StatPearls*, StatPearls Publishing, Treasure Island (FL), **2022**.
[11] R. Kanasty, J. R. Dorkin, A. Vegas, D. Anderson, *Nat. Mater.* **2013**, *12*, 967.
[12] C. Chakraborty, A. R. Sharma, G. Sharma, C. G. P. Doss, S.-S. Lee, *Mol. Ther. Nucleic Acids* **2017**, *8*, 132.
[13] X. Zhang, V. Goel, G. J. Robbie, *J. Clin. Pharmacol.* **2020**, *60*, 573.
[14] Z. Hejdankova, V. Vanek, F. Sedlak, J. Prochazka, A. Diederichs, S. Kereïche, B. Novotna, M. Budesinsky, G. Birkus, K. Grantz Saskova, P. Cigler, *Adv. Funct. Mater.* **2021**, *31*, 2101391.
[15] Y. Xiao, K. Shi, Y. Qu, B. Chu, Z. Qian, *Mol. Ther. - Methods Clin. Dev.* **2019**, *12*, 1.
[16] J. Hofman, M. Buncek, R. Haluza, L. Streinz, M. Ledvina, P. Cigler, *Macromol. Biosci.* **2013**, *13*, 167.
[17] M. Chen, X.-Q. Zhang, H. B. Man, R. Lam, E. K. Chow, D. Ho, *J. Phys. Chem. Lett.* **2010**, *1*, 3167.
[18] A. Alhaddad, M.-P. Adam, J. Botsoa, G. Dantelle, S. Perruchas, T. Gacoin, C. Mansuy, S. Lavielle, C. Malvy, F. Treussart, J.-R. Bertrand, *Small* **2011**, *7*, 3087.
[19] S. Claveau, M. Kindermann, A. Papine, Z. V. Díaz-Riascos, X. Délen, P. Georges, R. López-Alemany, Ò. M. Tirado, J.-R. Bertrand, I. Abasolo, P. Cigler, F. Treussart, *Nanoscale* **2021**, *13*, 9280.
[20] D. G. Lim, N. Rajasekaran, D. Lee, N. A. Kim, H. S. Jung, S. Hong, Y. K. Shin, E. Kang, S. H. Jeong, *ACS Appl. Mater. Interfaces* **2017**, *9*, 31543.
[21] S. Claveau, É. Nehlig, S. Garcia-Argote, S. Feuillastre, G. Pieters, H. A. Girard, J.-C. Arnault, F. Treussart, J.-R. Bertrand, *Nanomaterials* **2020**, *10*, 553.
[22] K. Turcheniuk, V. N. Mochalin, *Nanotechnology* **2017**, *28*, 252001.
[23] N. Nunn, M. Torelli, G. McGuire, O. Shenderova, *Curr. Opin. Solid State Mater. Sci.* **2017**, *21*, 1.
[24] P. Reineck, D. W. M. Lau, E. R. Wilson, K. Fox, M. R. Field, C. Deeleepojananan, V. N. Mochalin, B. C. Gibson, *ACS Nano* **2017**, *11*, 10924.
[25] J. Mikesova, D. Miliaieva, P. Stenclova, M. Kindermann, T. Vuckova, M. Madlikova, M. Fabry, V. Veverka, J. Schimer, P. Krejci, S. Stehlik, P. Cigler, *Carbon* **2022**, *195*, 372.
[26] J. Wehling, R. Dringen, R. N. Zare, M. Maas, K. Rezwan, *ACS Nano* **2014**, *8*, 6475.

[27] D.-K. Lee, S. V. Kim, A. N. Limansubroto, A. Yen, A. Soundia, C.-Y. Wang, W. Shi, C. Hong, S. Tetradis, Y. Kim, N.-H. Park, M. K. Kang, D. Ho, *ACS Nano* **2015**, *9*, 11490.
[28] L. Balek, M. Buchtova, M. Kunova Bosakova, M. Varecha, S. Foldynova-Trantirkova, I. Gudernova, I. Vesela, J. Havlik, J. Neburkova, S. Turner, M. A. Krzyscik, M. Zakrzewska, L. Klimaschewski, P. Claus, L. Trantirek, P. Cigler, P. Krejci, *Biomaterials* **2018**, *176*, 106.
[29] T. Rendler, J. Neburkova, O. Zemek, J. Kotek, A. Zappe, Z. Chu, P. Cigler, J. Wrachtrup, *Nat. Commun.* **2017**, *8*, 14701.
[30] G. Petrini, G. Tomagra, E. Bernardi, E. Moreva, P. Traina, A. Marcantoni, F. Picollo, K. Kvaková, P. Cígler, I. P. Degiovanni, V. Carabelli, M. Genovese, *Adv. Sci.* **2022**, *9*, 2202014.
[31] J. Barton, M. Gulka, J. Tarabek, Y. Mindarava, Z. Wang, J. Schimer, H. Raabova, J. Bednar, M. B. Plenio, F. Jelezko, M. Nesladek, P. Cigler, *ACS Nano* **2020**, *14*, 12938.
[32] L. Nie, A. C. Nusantara, V. G. Damle, M. V. Baranov, M. Chipaux, C. Reyes-San-Martin, T. Hamoh, C. P. Epperla, M. Guricova, P. Cigler, G. van den Bogaart, R. Schirhagl, *Nano Lett.* **2022**, *22*, 1818.
[33] A. Sigaeva, A. Hochstetter, S. Bouyim, M. Chipaux, M. Stejfova, P. Cigler, R. Schirhagl, *Small* **2022**, *18*, 2201395.
[34] T. Zhang, G. Pramanik, K. Zhang, M. Gulka, L. Wang, J. Jing, F. Xu, Z. Li, Q. Wei, P. Cigler, Z. Chu, *ACS Sens.* **2021**, *6*, 2077.
[35] I. Rehor, P. Cigler, *Diam. Relat. Mater.* **2014**, *46*, 21.
[36] S.-J. Yu, M.-W. Kang, H.-C. Chang, K.-M. Chen, Y.-C. Yu, *J. Am. Chem. Soc.* **2005**, *127*, 17604.
[37] T.-C. Hsu, K.-K. Liu, H.-C. Chang, E. Hwang, J.-I. Chao, *Sci. Rep.* **2014**, *4*, 5004.
[38] K. Kvakova, M. Ondra, J. Schimer, M. Petrik, Z. Novy, H. Raabova, M. Hajduch, P. Cigler, *Adv. Funct. Mater.* **2022**, *32*, 2109960.
[39] J. Neburkova, J. Vavra, P. Cigler, *Curr. Opin. Solid State Mater. Sci.* **2017**, *21*, 43.
[40] I. Rehor, J. Slegerova, J. Kucka, V. Proks, V. Petrakova, M.-P. Adam, F. Treussart, S. Turner, S. Bals, P. Sacha, M. Ledvina, A. M. Wen, N. F. Steinmetz, P. Cigler, *Small* **2014**, *10*, 1106.
[41] I. Rehor, H. Mackova, S. K. Filippov, J. Kucka, V. Proks, J. Slegerova, S. Turner, G. Van Tendeloo, M. Ledvina, M. Hruby, P. Cigler, *ChemPlusChem* **2014**, *79*, 21.
[42] R. Barbey, L. Lavanant, D. Paripovic, N. Schüwer, C. Sugnaux, S. Tugulu, H.-A. Klok, *Chem. Rev.* **2009**, *109*, 5437.
[43] X.-Q. Zhang, M. Chen, R. Lam, X. Xu, E. Osawa, D. Ho, *Acs Nano* **2009**, *3*, 2609.
[44] S. Lukowski, E. Neuhoferova, M. Kinderman, R. Krivohlava, A. Mineva, V. Petrakova, V. Benson, *J. Biomed. Nanotechnol.* **2018**, *14*, 946.
[45] I. Badea, Kaur, Michel, Chitanda, Maley, Yang, Borondics, Verrall, *Int. J. Nanomedicine* **2012**, 3851.
[46] V. Petrakova, V. Benson, M. Buncek, A. Fiserova, M. Ledvina, J. Stursa, P. Cigler, M. Nesladek, *Nanoscale* **2016**, *8*, 12002.
[47] M. Mumtaz, N. Hussain, S. Salam, M. Bilal, *J. Mater. Sci.* **2022**, *57*, 8064.
[48] S. R. Hemelaar, A. Nagl, F. Bigot, M. M. Rodríguez-García, M. P. de Vries, M. Chipaux, R. Schirhagl, *Microchim. Acta* **2017**, *184*, 1001.
[49] X. Kong, L. C. L. Huang, S.-C. V. Liau, C.-C. Han, H.-C. Chang, *Anal. Chem.* **2005**, *77*, 4273.
[50] P. Zhang, J. Yang, W. Li, W. Wang, C. Liu, M. Griffith, W. Liu, *J. Mater. Chem.* **2011**, *21*, 7755.
[51] G. Fritz, V. Schädler, N. Willenbacher, N. J. Wagner, *Langmuir* **2002**, *18*, 6381.
[52] K. Kunath, A. von Harpe, D. Fischer, H. Petersen, U. Bickel, K. Voigt, T. Kissel, *J. Control. Release Off. J. Control. Release Soc.* **2003**, *89*, 113.
[53] I. R. Hill, M. C. Garnett, F. Bignotti, S. S. Davis, *Biochim. Biophys. Acta* **1999**, *1427*, 161.
[54] S. Agarwal, Y. Zhang, S. Maji, A. Greiner, *Mater. Today* **2012**, *15*, 388.
[55] M. Neu, D. Fischer, T. Kissel, *J. Gene Med.* **2005**, *7*, 992.

[56] D. Fischer, T. Bieber, Y. Li, H.-P. Elsässer, T. Kissel, *Pharm. Res.* **1999**, *16*, 1273.
[57] Z. Rezvani Amin, M. Rahimizadeh, H. Eshghi, A. Dehshahri, M. Ramezani, *Iran. J. Basic Med. Sci.* **2013**, *16*, 150.
[58] J. W. Lee, S. Lee, S. Jang, K. Y. Han, Y. Kim, J. Hyun, S. K. Kim, Y. Lee, *Mol. Biosyst.* **2013**, *9*, 1004.
[59] N. Prabhakar, T. Näreoja, E. von Haartman, D. Ş. Karaman, H. Jiang, S. Koho, T. A. Dolenko, P. E. Hänninen, D. I. Vlasov, V. G. Ralchenko, S. Hosomi, I. I. Vlasov, C. Sahlgren, J. M. Rosenholm, *Nanoscale* **2013**, *5*, 3713.
[60] L. Cheng, Y. Li, X. Zhai, B. Xu, Z. Cao, W. Liu, *ACS Appl. Mater. Interfaces* **2014**, *6*, 20487.
[61] L. Zhao, Y. Nakae, H. Qin, T. Ito, T. Kimura, H. Kojima, L. Chan, N. Komatsu, *Beilstein J. Org. Chem.* **2014**, *10*, 707.
[62] A. Akinc, W. Querbes, S. De, J. Qin, M. Frank-Kamenetsky, K. N. Jayaprakash, M. Jayaraman, K. G. Rajeev, W. L. Cantley, J. R. Dorkin, J. S. Butler, L. Qin, T. Racie, A. Sprague, E. Fava, A. Zeigerer, M. J. Hope, M. Zerial, D. W. Y. Sah, K. Fitzgerald, M. A. Tracy, M. Manoharan, V. Koteliansky, A. de Fougerolles, M. A. Maier, *Mol. Ther. J. Am. Soc. Gene Ther.* **2010**, *18*, 1357.
[63] I. Lynch, K. A. Dawson, *Nano Today* **2008**, *3*, 40.
[64] E. Blanco, H. Shen, M. Ferrari, *Nat. Biotechnol.* **2015**, *33*, 941.
[65] A. Zintchenko, A. Philipp, A. Dehshahri, E. Wagner, *Bioconjug. Chem.* **2008**, *19*, 1448.
[66] R. A. Jones, M. H. Poniris, M. R. Wilson, *J. Controlled Release* **2004**, *96*, 379.
[67] J. Kopecek, H. Bazilova, *Eur. Polym. J.* **1973**, *9*, 7.
[68] J. Kopecek, P. Kopeckova, *Adv. Drug Deliv. Rev.* **2010**, *62*, 122.
[69] J. Slegerova, M. Hajek, I. Rehor, F. Sedlak, J. Stursa, M. Hruby, P. Cigler, *Nanoscale* **2015**, *7*, 415.
[70] J. Neburkova, F. Sedlak, J. Zackova Suchanova, L. Kostka, P. Sacha, V. Subr, T. Etrych, P. Simon, J. Barinkova, R. Krystufek, H. Spanielova, J. Forstova, J. Konvalinka, P. Cigler, *Mol. Pharm.* **2018**, *15*, 2932.
[71] J. Neburkova, M. Hajek, I. Rehor, J. Schimer, F. Sedlak, J. Stursa, M. Hruby, P. Cigler, In *Integrin Targeting Systems for Tumor Diagnosis and Therapy*, Humana Press, **2018**, pp. 169–189.
[72] P. Kovaříček, M. Cebecauer, J. Neburková, J. Bartoň, M. Fridrichová, K. A. Drogowska, P. Cigler, J.-M. Lehn, M. Kalbac, *ACS Nano* **2018**, *12*, 7141.
[73] R. Kumar, B. Yang, J. Barton, M. Stejfova, A. Schäfer, M. König, P. Knittel, P. Cigler, M. Hirtz, *Adv. Mater. Interfaces* **2022**, *9*, 2201453.
[74] M. Henze, D. Mädge, O. Prucker, J. Rühe, *Macromolecules* **2014**, *47*, 2929.
[75] X. Zhang, C. Fu, L. Feng, Y. Ji, L. Tao, Q. Huang, S. Li, Y. Wei, *Polymer* **2012**, *53*, 3178.
[76] J. Buffle, K. J. Wilkinson, S. Stoll, M. Filella, J. Zhang, *Environ. Sci. Technol.* **1998**, *32*, 2887.
[77] G. V. Lowry, R. J. Hill, S. Harper, A. F. Rawle, C. O. Hendren, F. Klaessig, U. Nobbmann, P. Sayre, J. Rumble, *Environ. Sci. Nano* **2016**, *3*, 953.
[78] A. V. Delgado, F. González-Caballero, R. J. Hunter, L. K. Koopal, J. Lyklema, *J. Colloid Interface Sci.* **2007**, *309*, 194.
[79] E. Hotze, S. Louie, S. Lin, M. Wiesner, G. Lowry, *Environ. Chem.* **2014**, *11*, 257.
[80] J. T. Paci, H. B. Man, B. Saha, D. Ho, G. C. Schatz, *J. Phys. Chem. C* **2013**, *117*, 17256.
[81] R. Krivohlava, E. Neuhoferova, K. Q. Jakobsen, V. Benson, *Nanomaterials* **2019**, *9*, 866.
[82] E. M. Hotze, T. Phenrat, G. V. Lowry, *J. Environ. Qual.* **2010**, *39*, 1909.
[83] J. Suh, H.-J. Paik, B.-K. Hwang, *Ionization of poly(ethylenimine) and poly(allylamine) at various pH's*, **1994**.
[84] R. McElreath, *Statistical rethinking: a Bayesian course with examples in R and Stan*, 1st Edition., CRC Press/Taylor & Francis Group, Boca Raton, **2016**.

[85] Majer, Jan, Kindermann, Marek, Pinkas, Dominik, Chvatil, David, Cigler, Petr, Libusova, Lenka, **2023**, https://www.biorxiv.org/content/10.1101/2023.11.02.564900v1.
[86] J. I. Cutler, E. Auyeung, C. A. Mirkin, *J. Am. Chem. Soc.* **2012**, *134*, 1376.
[87] C. H. J. Choi, L. Hao, S. P. Narayan, E. Auyeung, C. A. Mirkin, *Proc. Natl. Acad. Sci.* **2013**, *110*, 7625.
[88] E. Neuhoferova, M. Kindermann, M. Buzgo, K. Vocetkova, D. Panek, P. Cigler, V. Benson, **2023**, https://www.biorxiv.org/content/10.1101/2023.11.06.565704v1.
[89] S. K. Filippov, P. Chytil, P. V. Konarev, M. Dyakonova, ChristineM. Papadakis, A. Zhigunov, J. Plestil, P. Stepanek, T. Etrych, K. Ulbrich, D. I. Svergun, *Biomacromolecules* **2012**, *13*, 2594.
[90] O. Cakmak, C. Elbuken, E. Ermek, A. Mostafazadeh, I. Baris, B. Erdem Alaca, I. H. Kavakli, H. Urey, *Methods San Diego Calif* **2013**, *63*, 225.
[91] A. K. Pal, I. Aalaei, S. Gadde, P. Gaines, D. Schmidt, P. Demokritou, D. Bello, *ACS Nano* **2014**, *8*, 9003.
[92] Y. Li, J. Sun, C.-K. Tang, H.-Y. Shum, *ACM Trans. Graph.* **2004**, *23*, 303.
[93] H. Wickham, R. François, L. Henry, K. Müller, *dplyr: A Grammar of Data Manipulation*, **2022**.
[94] A. de Vries, B. D. Ripley, *ggdendro: Create Dendrograms and Tree Diagrams Using "ggplot2,"* **2022**.
[95] A. Vehtari, J. Gabry, M. Magnusson, Y. Yao, P.-C. Bürkner, T. Paananen, A. Gelman, *loo: Efficient leave-one-out cross-validation and WAIC for Bayesian models*, **2022**.
[96] B. Schloerke, D. Cook, J. Larmarange, F. Briatte, M. Marbach, E. Thoen, A. Elberg, J. Crowley, *GGally: Extension to "ggplot2,"* **2021**.
[97] J. Gabry, T. Mahr, *bayesplot: Plotting for Bayesian Models*, **2022**.
[98] H. Wickham, *ggplot2: Elegant Graphics for Data Analysis*, Springer-Verlag New York, **2016**.
[99] R Core Team, *R: A Language and Environment for Statistical Computing*, R Foundation for Statistical Computing, Vienna, Austria, **2021**.
[100] D. Makowski, M. S. Ben-Shachar, D. Lüdecke, *J. Open Source Softw.* **2019**, *4*, 1541.
[101] P.-C. Bürkner, *J. Stat. Softw.* **2017**, *80*, 1.
[102] C. O. Wilke, *cowplot: Streamlined Plot Theme and Plot Annotations for "ggplot2,"* **2020**.

Table of Contents

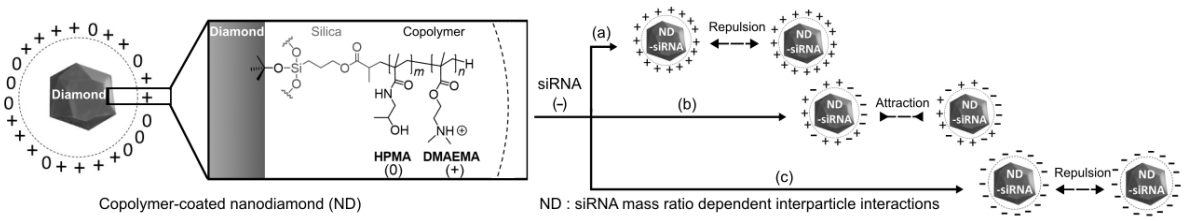

The study presents a non-viral vector for siRNA based on nanodiamond coated with a novel copolymer with tunable charge density. The properties of the vector are optimized by several physicochemical variables and polymer composition, and correlated with biological efficacy, cytotoxicity and cell proliferation. This colloidal and biologically stable siRNA delivery tool demonstrates potential for siRNA transfection and RNA interference-based therapeutics.